Altered ciliary morphofunction in the oviductal infundibulum of systemic autoimmune disease-prone MRL/MpJ-*Fas*$^{lpr/lpr}$ mice

Authors: Marina Hosotani[1, 2*], Osamu Ichii[2], Teppei Nakamura[2, 3], Md. Abdul Masum[2], Yuki Otani[2], Yaser Hosny Ali Elewa[2, 4], Yasuhiro Kon[2]

Addresses: [1]Laboratory of Anatomy, School of Veterinary Medicine, Rakuno Gakuen University, Ebetsu, Hokkaido 069-8501, Japan

[2]Laboratory of Anatomy, Department of Basic Veterinary Science, Faculty of Veterinary Medicine, Hokkaido University, Sapporo, Hokkaido 060-0818, Japan

[3]Section of Biomedical Science, Chitose Laboratory, Japan Food Research Laboratories, Chitose, Hokkaido 066-0052, Japan

[4]Department of Histology and Cytology, Faculty of Veterinary Medicine, Zagazig University, Zagazig 44519, Egypt

[*]**Corresponding author: Marina Hosotani, DVM.,**

Laboratory of Anatomy, School of Veterinary Medicine, Rakuno Gakuen University, Midorimachi 582, Bunkyodai, Ebetsu 069-8501, Japan.

Tel & Fax: +81-11-388-4763

Email: m-hosotani@rakuno.ac.jp

Email: Osamu Ichii; ichi-o@vetmed.hokudai.ac.jp, Teppei Nakamura; nakamurate@vetmed.hokudai.ac.jp, Md. Abdul Masum; Masum@vetmed.hokudai.ac.jp, Yuki Otani; yukiotani35@vetmed.hokudai.ac.jp, Yaser Hosny Ali Elewa; y-elewa@vetmed.hokudai.ac.jp, Yasuhiro Kon; y-kon@vetmed.hokudai.ac.jp.

Abbreviations

CBF, ciliary beat frequency

COC, cumulus oocyte complex

D-MEM, Dulbecco's Modified Eagle's Medium (high glucose) with L-Glutamine and phenol red

dsDNA, double-stranded DNA

Fas, Fas cell surface death receptor

hCG, human chorionic gonadotropin

lpr, lymphoproliferation

MRL/+, MRL/MpJ

MRL/lpr, MRL/MpJ-*Fas*$^{lpr/lpr}$

OO, ovulated oocyte

PB, phosphate buffer

PBS, phosphate buffered saline

PCD, primary ciliary dyskinesia

PFA, paraformaldehyde

PMSG, pregnant mare serum gonadotropin

PUR, oocyte pick-up rate

ROI, region of interest

40 S/B, ratio of spleen weight to body weight

41 TEM, transmission electron microscope

Abstract

According to our previous reports, impaired oocyte pick-up was observed in the oviductal infundibulum of autoimmune disease (AD) mouse model, suggesting a relationship between female infertility and AD. This study examined the relationship between AD and infundibulum morphofunction by focusing on the epithelial cilia. Healthy MRL/MpJ and AD-prone MRL/MpJ-*Fas*$^{lpr/lpr}$ mice were examined at 3 and 6 months of age, representing early and late disease stages, respectively. Oocyte pick-up indices decreased with AD progression indicated by splenomegaly, autoantibody production, and increased T-cell counts of infundibulum mucosa in MRL/MpJ-*Fas*$^{lpr/lpr}$ mice. Ciliary beating frequency (CBF) and height in the infundibulum were faster and higher in MRL/MpJ-*Fas*$^{lpr/lpr}$ mice than in MRL/MpJ mice at the early AD stages, although the absolute CBF values were lower at the late AD stage. At late stage, ciliary height did not differ between mouse lines, but the morphological index of cilia beating direction indicated randomized patterns in MRL/MpJ-*Fas*$^{lpr/lpr}$ mice. The tracheal mucosa was also examined as a representative example of cilia morphology; its CBF decreased at late AD stage in MRL/MpJ-*Fas*$^{lpr/lpr}$, however, there were no AD-related morphological changes. Our results demonstrate altered cilia motility in systemic and reproductive organs, with such morphological changes of the infundibulum likely impairing function, including oocyte pick-up.

Key Words: Oocyte pick-up, ciliary beat frequency, inflammation, lupus, trachea

Introduction

In mammals, a close relationship between female infertility and immune abnormalities, including infection and autoimmune diseases, has been reported. For example, human patients with autoimmune diseases that are local, such as autoimmune hepatitis or autoimmune thyroid disease, or systemic, like multiple sclerosis and celiac disease, have increased risks of infertility (Carp and Selmi 2012). Autoimmune diseases are believed to affect the function of the female reproductive tract when the failure of immune control alters the endocrine profile, metabolism, sex hormone response, and tissue morphology, leading to failure of ovulation, fertilization and implantation (Luborsky 2002; Haller-Kikkatalo et al. 2012; Sen et al. 2014; Otani et al. 2015; Hosotani et al. 2018).

Approximately 20-30% of female infertility cases are suggested to be caused by problems associated with oviductal dysfunction (Nagata et al. 2004; Roupa Z et al. 2009). Oviduct morphofunction can be affected by the condition of surrounding tissues. For example, the spread of inflammation in peritoneal cavity and/or uterus to the oviductal lumen induces oviductal swelling and/or adhesion, leading to luminal interruption (Magdy and El-Bahrawy 2014). Peritubal adhesions or damage to oviduct lining resulted from inflammatory conditions can impair tubal mobility, sperm and embryo transport, and oocyte pick-up (Magdy and El-Bahrawy 2014). In addition, in Holstein repeat breeder cows, oviductal luminal blockage seriously impairs fertility

(Sawamukai et al. 2014).

One of the primary functions of the oviduct in reproduction is oocyte pick-up, in which it takes oocytes produced in the ovary into the oviductal lumen (Huang et al. 1997), while infundibulum dysfunction prevents oocyte fertilization. One theory regarding the underlying mechanism of oocyte pick-up is that well-controlled ciliary beating on the infundibulum epithelium transports oocytes into the lumen (Shi et al. 2011), although the actual physical mechanism of oocyte pick-up is not fully understood.

We previously found that the autoimmune disease model mice line MRL/MpJ-*Fas*$^{lpr/lpr}$ (MRL/lpr) shows an oocyte pick-up disorder and abnormal morphology of the oviductal infundibulum and T-cell inflammation in the oviductal epithelium and lamina propria (Hosotani et al. 2018). MRL/lpr mice bear the lymphoproliferation mutation (*lpr*) in the Fas cell surface death receptor (*Fas*) gene (Santiago-Raber et al. 2004), causing severe phenotypes associated with spontaneous systemic autoimmune disease, including splenomegaly, arthritis, vasculitis, and autoimmune glomerulonephritis, which are similar symptoms as those from human systemic lupus erythematosus (Andrews et al. 1978). Our previous study also indicated that the progression of a systemic autoimmune abnormality or the local infiltration of immune cells into the oviductal mucosa in MRL/lpr mice negatively impact oocyte pick-up (Hosotani et al. 2018). However, it is still unknown whether the infundibulum ciliary functions driving the healthy oocyte pick-up are

impaired by these immunological disorders or other endogenous factors.

In this study, we examined the morphofunction of ciliated epithelial cells on the oviductal infundibulum in MRL/lpr mice to determine the effects of the autoimmune abnormalities on the cilia regulating oocyte pick-up. In addition to the oviduct, we also examined the ciliary morphofunction of tracheal ciliated epithelial cells as a representative organ for motile cilia possession and compared their morphology with that of the oviduct. We also propose the novel pathological theory that altered ciliary function triggered by an autoimmune abnormality contributes to oocyte pick-up disorder and note interesting similarities of ciliary morphofunction in the oviduct and trachea.

Material and Methods

Animals

Animal experimentation was approved by the Institutional Animal Care and Use Committee of the Graduate School of Veterinary Medicine, Hokkaido University (Approval No. 15-0079). Experimental animals were handled in accordance with the Guide for the Care and Use of Laboratory Animals, Graduate School of Veterinary Medicine, Hokkaido University (approved by the Association for Assessment and Accreditation of Laboratory Animal Care International). Female MRL/MpJ (MRL/+) and MRL/lpr mice at 3 and 6 months of age were obtained from Japan

115 SLC, Inc. (Hamamatsu, Shizuoka, Japan). The MRL strains were derived mainly from the LG/J
116 strain, with contributions from AKR/J, C3H/Di, and C57BL/6J strains (Andrews et al. 1978). It
117 has been reported that MRL/+ mice exhibit regular estrous cyclicity, with each cycle lasting 4 to 7
118 days until 11 months of age. On the other hand, MRL/lpr mice were found to lose estrous cyclicity
119 after 6 months, as characterized by a prolonged diestrus period and a shortened estrus period (Otani
120 et al. 2015). The mice were housed in plastic cages in groups at 18°C to 26°C under a 12 h
121 light/dark cycle and had free access to commercial diet and water. Pregnant mare serum
122 gonadotropin (PMSG, ASKA Animal Health Co., Ltd., Minato, Tokyo, Japan) was injected
123 intraperitoneally in mice (200 µl of 37.5 IU/ml gonadotropin per mouse). After 48 h of PMSG
124 injection, mice were injected intraperitoneally with the same dose of human chorionic
125 gonadotropin (hCG, ASKA Animal Health Co., Ltd.). The procedure for superovulation treatment
126 was based on that described in a previous report (Takeo et al. 2008).
127 Twenty-four hours after hCG injection, all mice were euthanized by cutting the carotid artery
128 or cervical dislocation under deep anesthesia induced using a mixture of medetomidine (0.3
129 mg/kg), midazolam (4 mg/kg), and butorphanol (5 mg/kg).
130
131 ***Evaluation of autoimmune disease condition***
132 Spleen were collected from euthanized mice in order to measure the ratio of spleen weight to

body weight, which serves as a marker of an autoimmune disease. In addition, anti-double strand DNA (dsDNA) antibody levels in mice serum were measured using the LBIS anti dsDNA-Mouse ELISA kit (FUJIFILM Wako Pure Chemical Co., Ltd., Osaka, Osaka, Japan) according to the manufacturer's instructions.

Evaluation of oocyte pick-up by the oviduct

Oocyte pick-up rate (PUR) was calculated following our previous method (Hosotani et al. 2018). Briefly, the ovaries and oviductal ampulla were collected from mice and immediately placed in 0.01 M phosphate buffered saline (PBS). The cumulus oocyte complexes (COCs) present in the ampulla were pushed out into a glass dish with 0.01 M PBS and counted. Ovaries were fixed with 4% paraformaldehyde (PFA) at 4°C overnight, embedded in paraffin, and cut into 10 µm-thick whole serial sections, which were used for the histological counting of ovulated oocytes (OOs) from the ovaries. PUR was then calculated as follows: PUR (%) = 100 × number of COCs / number of OOs.

Histological analysis

Mice oviducts and tracheas were collected and fixed with 4% PFA at 4°C overnight, embedded in paraffin, and cut into 3 µm-thick sections, which were then used for hematoxylin-

151 eosin staining and immunohistochemistry. Sections were incubated in 20 mM Tris-HCl (pH 9.0)
152 for 20 min at 105°C. Sections were then soaked in methanol containing 0.3% H_2O_2, blocked in
153 10% normal goat serum (SABPRO Kit, Nichirei Co., Ltd., Chuou, Tokyo, Japan) for 30 min at
154 room temperature were incubated with rabbit anti-CD3 (Nichirei Co., Ltd.) at 4°C overnight. After
155 washing three times in PBS, sections were incubated with biotin-conjugated goat anti-rabbit IgG
156 antibody (SABPRO Kit, Nichirei Co., Ltd.) for 30 min, washed, and incubated with streptavidin-
157 biotin complex (SABPRO Kit, Nichirei Co., Ltd.) for 30 min at room temperature. Sections were
158 then incubated with 3, 3' –diaminobenzidine tetrahydrochloride- H_2O_2 solution, and lightly
159 stained with hematoxylin.
160
161 ***Ciliary beat frequency (CBF) measurement***
162 *Sample collection and movie recording*
163 Ciliary beating was analyzed by a program developed by Dr. Jason J. Chen(Chen et al. 2016).
164 The collected oviductal and tracheal specimens of the superovulated mice were kept in D-MEM
165 (high glucose) with L-glutamine and phenol red (D-MEM) (FUJIFILM Wako Pure Chemical Co.,
166 Ltd.) at 37°C. Using a stereoscope, the infundibulum was detached from the oviduct. The excess
167 soft tissue was removed via microdissection and the trachea was sectioned into 1 mm^2 to 4 mm^2
168 pieces, which were then incubated for 30 min in D-MEM at 37°C and placed onto slides for

observation (Supplementary Fig. S1). As shown in Supplementary Fig. S1a, the oviductal infundibulum was put into a chamber with D-MEM (Matsunami Glass Industry Co., LTD., Kishiwada, Osaka, Japan), following a published method previously used to study CBF in oviducts(Shi et al. 2011). Trachea tissue pieces were also put under cover slips in D-MEM (Supplementary Fig. S1b). Ciliary movements were observed using a phase contrast microscope (BX50, Olympus Co., Ltd., Shinjuku, Tokyo, Japan) and recorded through the ocular lens using an iPhone 6S (Apple Inc., Cupertino, California, U.S.A.) at 240 frames per second.

Data analysis

The program used for CBF data analysis was written in MATLAB (MathWorks Inc., Natick, Massachusetts, U.S.A.) was used for CBF data analysis as described previously (Chen et al. 2016). A 3-second video was isolated from each recording and regions of interest (ROIs) selected according to histologic findings. Power spectrum graphs were then generated to determine the CBF of the samples. The mean CBF values for each individual specimen were obtained by analyzing more than 100 ROIs and averaging CBF values of those ROIs.

Ultrastructural analysis

For transmission electron microscope (TEM) analysis, perfusion fixation was performed on

3- and 6-month old superovulated MRL/+ and MRL/lpr mice. The vena cava was cut and released under deep anesthesia and 20 ml of PBS and half-Karnovsky's fixing solution (2.5% glutaraldehyde, 2% PFA, 0.1 M phosphate buffer (PB), pH 7.4) perfused from the left ventricle to the whole body. The detached infundibulum from the oviducts and the trachea beneath the isthmus of the thyroid grand were post-fixed with 1% osmium tetroxide in 0.1 M PB for 2 hours at 4°C. Specimens were dehydrated using a graded alcohol series and embedded in epoxy resin (Quetol 812 Mixture; Nisshin EM CO., Ltd., Shinjuku, Tokyo, Japan). The epoxy blocks were cut into 60 nm-thick sections, stained with uranyl acetate and lead citrate, and examined via a JEM-1210 microscope (JEOL Ltd., Akishima, Tokyo, Japan).

The orientation of the ciliary central microtubules was measured as previously described(Guirao et al. 2010). The ciliary orientation is defined by the plane formed by the central tubules and is used to estimate ciliary beat direction by measuring the angle between the central tubule plane and a reference line(Rautiainen et al. 1986). Reference lines were drawn through the central pairs of microtubules using Image J software (National Institutes of Health, Bethesda, MD, USA). The mean vector length (r_{cell}) represents the circular variance of these angles within the cell. In one specimen, more than 10 cells which have more than 10 cilia clearly expressing pairs of central microtubules were chosen and analyzed for calculating of the average r_{cell} in each specimen. The ciliary height on the ciliated epithelial cells was defined as the distance between "the upper

end of the cilia" and "luminal surface of the cell." The height was measured using Image J on more than 10 ciliated cells within one specimen.

Statistical analysis

Results were expressed as mean ± standard error (s.e.m) and statistically analyzed in a non-parametric manner. Data between two groups were compared using the Mann-Whitney *U*-test ($P < 0.05$). Correlations between two parameters were analyzed using Spearman's correlation test ($P < 0.05$). The statistical analysis was conducted in JMP 14.2.0 (SAS Institute Inc., Cary, North Carolina, USA).

Results

Autoimmune disease status, altered ovulation, and oocyte pick-up in MRL/lpr mice

As described in previous studies (Hosotani et al. 2018), MRL/lpr mice showed both significantly greater splenomegaly and significantly higher serum levels of anti-dsDNA antibody at 3 and 6 months of age compared with MRL/+ mice (Fig. 1a and b). In addition, the COC, OO, and PUR values in 6-month-old MRL/lpr mice (5.36 ± 0.95, 7.18 ± 1.46, and 76.93 ± 6.33 %, respectively) were significantly lower as compared with those of 3-month-old MRL/lpr mice (41.63 ± 5.47, 43.57 ± 6.35, and 100.69 ± 3.31 %, respectively) and with those of 6-month-old

MRL/+ mice (20.75 ± 1.82, 20.63 ± 1.60, and 101.10 ± 5.11 %, respectively) (Fig. 1c-e). Furthermore, in MRL/+ mice, significant age-associated reductions were observed for COCs and OOs, but not in PUR (41.63 ± 2.98, 39.29 ± 2.02, and 101.73 ± 3.83 % in 3-month-old MRL/+ mice, respectively). These results were similar with our previous report (Hosotani et al. 2018) and were used to examine the correlations among autoimmune abnormality, ovulation and oocyte pick-up function, and ciliary function. Further, correlation analysis between the PUR and the number of COCs and OOs was performed to examine the relationship between oocyte pick-up and ovulation (Table1). In all of the mice included in the analysis and MRL/lpr mice, PUR showed significant positive correlations with both the COCs ($P < 0.01$) and the OOs value ($P < 0.05$).

Histology and inflammation of infundibulum in the oviducts of MRL/lpr mice

The oviductal epithelium mainly consists of ciliated epithelial cells and secretory cells (Peters 1986; Crow et al. 1994). Six-month-old MRL/lpr mice showed a higher number of secretory cells covering the surface of the infundibulum epithelium compared to both MRL/+ mice at same age and 3-month-old MRL/lpr mice (Fig. 2a-a'''). Under the light microscope, there were no clear histological differences in the morphology of ciliated epithelial cells among the groups. Finally, as observed in our previous study (Hosotani et al. 2018), there were much higher numbers of CD3-positive T-cells infiltrating the mucus and epithelium of the oviductal infundibulum in MRL/lpr

241 mice at 6 months compared to other groups examined (Fig. 2b-b’’’).

242

243 *Altered oviductal ciliary beating in MRL/lpr*

244 We recorded the ciliary beating frequency (CBF) using stereomicroscopy, and representative
245 still images from these movies are shown in Fig. 2c-c’’’ (with movies in Online Resource 1-4).
246 From these movies, MRL/lpr mice had significantly higher oviductal CBF in the infundibulum at
247 both 3 and 6 months (11.41 $\pm$ 0.09 Hz and 10.67 $\pm$ 0.21 Hz, respectively) compared to MRL/+
248 mice at each corresponding age (10.25 $\pm$ 0.27 Hz and 9.18 $\pm$ 0.37 Hz, respectively) (Fig. 2d).
249 Importantly, the oviductal CBF showed significant age-related decreases in MRL/lpr mice at 6
250 months.

251

252 *Altered direction of oviductal ciliary beating in MRL/lpr mice*

253 The ultrastructure of ciliated epithelial cells in the oviduct of MRL/+ and MRL/lpr at 3 and 6
254 months old is shown in Fig. 3a-h. No remarkable difference in cilia density was noted between
255 mouse strains and ages, but the oviductal ciliary height from the luminal top of the ciliated
256 epithelial cell seemed to be shortest in MRL/+ mice at 3 months old compared with other test
257 groups (Fig. 3a, c, e, and g, white arrows), which is also confirmed in the oviductal ciliated
258 epithelial cells in the HE-stained sections (Fig. 3a, c, e, and g, insets). Furthermore, the orientation

of the central microtubules in a cilium, which indicates the direction of cilial motion, was more randomized in 6 month MRL/lpr mice compared with the others (Fig. 3b, d, f, and h, white lines). However, there are no age-related differences in cilia composing structures in MRL/lpr mice (Fig. 3f and h, insets).

These morphological findings were summarized in Figure 4. At 3 months of age, the oviductal ciliary height from the luminal top of the ciliated epithelial cell was significantly higher in MRL/lpr than MRL/+ mice (Fig. 4a). While there was no change in the oviductal ciliary height of MRL/lpr mice with age, oviductal ciliary height of MRL/+ mice increased with aging. The variance values of the angles within a pair of central microtubules (Fig. 3b, d, f, and h, white lines) represents the cooperativity of the ciliary beating direction in a given cell. At 6 months of age, MRL/lpr mice showed significantly lower cilia alignment in the oviductal infundibulum than that in MRL/+ mice, while there were no differences among two strains at 3 months old (Fig. 4b).

Histology and inflammation of tracheal mucosa in MRL/lpr mice

In all examined mice, the tracheal mucosa was lined with ciliated pseudo-stratified columnar epithelium, and the epithelia heights were higher at 6 months old compared to 3 months old (Fig. 5a-a'''). Furthermore, in 6-month-old MRL/lpr mice, the non-ciliated cells and mononuclear cells beneath epithelium were frequently exposed, and a part of their epithelium was covered with mucin

277 layer (Fig. 5a’’’). As shown in Fig. 5b-b’’’, the mononuclear cells were CD3-positive and tended
278 to increase in number with aged mice, being particularly abundant in the lamina propria as well as
279 mucosal epithelium in 6-month-old MRL/lpr mice (Fig. 5b’’’).
280
281 *Altered systemic ciliary beating in MRL/lpr mice*
282 We also recorded the tracheal CBF as a representative tissue to indicate systemic cilia function
283 using stereomicroscopy and show representative still images from movie files in Fig. 5c-c’’’ (with
284 movies in Online Resource 5-8). While the tracheal CBF in 3-month-old MRL/lpr mice (8.16 ±
285 0.31 Hz) was significantly higher than that in MRL/+ of the same age (7.37 ± 0.17 Hz), the
286 tracheal CBF in MRL/lpr at 6 months (6.29 ± 0.41 Hz) was significantly lower than in MRL/+
287 of the same age (7.39 ± 0.26 Hz). Similar to oviductal CBF, MRL/lpr mice showed reduced
288 tracheal CBF with aging (Fig. 5d).
289
290 *Ultrastructure of tracheal ciliated epithelial cells in MRL/lpr mice*
291 The ciliary ultrastructure of the trachea of MRL/+ and MRL/lpr mice at 3 months and 6 months
292 of age showed no remarkable morphological differences among strains is shown in Fig. 6.
293 Furthermore, there were no significant differences in both the tracheal ciliary height and tracheal
294 cilia alignment among strains and ages (Fig. 7a and b).

295

296 *Autoimmune disease affects systemic ciliary function*

297 To examine the relationship between ciliary beating in both the oviduct and trachea and
298 autoimmune abnormality, ovulation, and oocyte pick-up, correlation analysis was performed for
299 these parameters (Table 2). First, in all of the mice included in the correlation analysis, the
300 oviductal CBF showed significant positive correlations with S/B ($P < 0.05$) and the serum anti-
301 dsDNA antibody levels ($P < 0.01$), which are indices of autoimmune disease. On the other hand,
302 in MRL/lpr mice, the oviductal and tracheal CBF showed significant negative correlations with
303 S/B ($P < 0.05$). Second, in MRL/+ mice, oviductal CBF correlated positively with the number of
304 COCs ($P < 0.05$). Additionally, all mice showed strong positive correlations between the tracheal
305 CBF and the number of COCs and OOs ($P < 0.001$), with MRL/lpr mice also showing a strong
306 positive correlation both the oviductal and tracheal CBF and the number of COCs and OOs ($P <$
307 0.001). Finally, tracheal CBF showed a significant positive correlation with PUR in all mice
308 examined ($P < 0.01$) and MRL/lpr mice ($P < 0.01$), with MRL/lpr mice also showing a significant
309 positive correlation between the oviductal and tracheal CBF ($P < 0.01$).

310 We also performed correlation analyses between ultrastructural morphological changes in both
311 the oviduct and trachea and autoimmune abnormalities (Table 3). The oviductal and tracheal r_{cell}
312 values showed significant strong positive correlations in MRL/lpr mice ($P < 0.001$) while in

313 MRL/+, the oviductal ciliary height correlated negatively with the S/B ratio ($P < 0.05$).

314

315 **Discussion**

316 As reported in previous studies (Otani et al. 2015; Hosotani et al. 2018) and the present study,
317 female MRL/lpr mice develop systemic autoimmune disease at the age of 3 months, which
318 becomes more severely exacerbated at 6 months of age. In MRL/lpr mice that developed severe
319 autoimmune diseases, a large number of immune cells infiltrated the oviductal and the tracheal
320 mucosa as reported for other systemic organs such as the ovaries, kidneys, lungs, skin, and liver
321 (Yang et al. 2003; Ichii et al. 2010; Otani et al. 2015; Elewa et al. 2017; Hosotani et al. 2018; Fang
322 et al. 2018). Both the healthy oviduct and trachea contain a heterogeneous population of innate
323 and adaptive immune cells, including T-cells (Ardighieri et al. 2014; Iwasaki et al. 2017). In the
324 mucosa, these T-cells play an important role in maintaining mucosal homeostasis and are involved
325 in inflammation regulation, tissue repair, and protection against infectious agents (Ardighieri et al.
326 2014). Therefore, it is suggested that the excess auto-reactive lymphoproliferation due to the
327 failure of negative selection of thymocytes by Fas protein disrupts the normal immune balance and
328 induces the infiltration of numerous T-cells in both oviduct and trachea of older MRL/lpr mice.

329 At 3 months, there was no difference in ovulation and oocyte pick-up indices between both
330 strains, but the oviductal epithelium of MRL/lpr mice had faster CBF and longer cilia compared

331 with MRL/+ mice. For each cell type there is a specific range of normal lengths for cilia, and even
332 slight deviations outside of this range are often sufficient to generate pathological phenotypes
333 (Avasthi and Marshall 2012). Mice lacking ciliary length control show female infertility because
334 the elongated cilia in the oviduct cannot maintain proper fluid flow leading to the tubal obstruction
335 (Niwa et al. 2012). While cilium elongated in MRL/+ mice with aging, ciliary elongation occurred
336 at an earlier age in MRL/lpr mice than MRL/+ mice. In addition, the inflammatory cytokine
337 stimulation produced during chronic inflammation induces the sustained elongation of primary
338 cilia, another type of cilia than examined in this study, and the subsequent loss of length regulation
339 function (Dummer et al. 2018). Although the direct effect and mechanism of ciliary elongation in
340 3-month-old MRL/lpr mice remains unclear, we propose that the faster oviductal CBF in MRL/lpr
341 mice might compensate for altered cilia function due to morphological changes and maintain
342 normal oocyte pick-up.

343 As reported previously (Hosotani et al. 2018), MRL/+ and MRL/lpr mice show decreased
344 ovulation with aging, with the latter showing a more remarkable decrease in ovulation as well as
345 oocyte pick-up. Furthermore, the oviducts of 6-month-old MRL/lpr mice showed decreased CBF,
346 lost ciliary cooperativity and progress autoimmune disease than 3-month-old MRL/lpr mice. In the
347 our previous study, the percentage of the ciliated epithelial cells covering the epithelium in the
348 infundibulum of MRL/lpr was lower at 6 months of age compared to 3 months (Hosotani et al.

2018). In addition, a previous study demonstrated that the infundibulum mucosa and the ovarian surface are closely associated with slow COCs release (Gordts et al. 1998). In addition, the process of the oocyte pick-up representatively comprises of both oviductal ciliary beating and the transient adhesion of COCs to the tips of cilia (Norwood et al. 1978), In fact, considering the strong correlation between “the number of OOs and COCs” and “the oviductal CBF and the PUR” in MRL/lpr mice, the interaction and adhesion of cumulus cells and cilia in the infundibulum epithelium likely play a key role in the pathological state of ovulation and oocyte pick-up dysfunction in MRL/lpr mice. Further, these results imply that oocytes or the cumulus cells themselves regulate oviductal ciliary function to promote healthy oocyte pick-up. We therefore considered that the severe morphofunctional changes of oviductal epithelium, in particular those of cilia, found in 6-month-old MRL/lpr mice would ultimately impair not only ovulation but also oocyte pick-up.

The oviductal CBF showed significant correlation with the extent of splenomegaly in all mice examined and MRL/lpr, indicating a relationship between autoimmune abnormality and ciliary function. MRL/+ mice exhibit autoimmune disease-associated abnormalities but have milder symptoms that manifest much later in life compared to MRL/lpr mice (Kanno et al. 1992). Several inflammatory factors are reported to potentially alter the CBF in both human oviduct and respiratory tracts in *ex vivo* experiments, including IL-6 (Papathanasiou et al. 2008), IL-4, IL-5,

IL-9, IL-13, IFN-ɤ (Grosse-Onnebrink et al. 2016), and platelet-activating factor (Klettke et al. 1999). Previous reports indicate that the high serum levels of IL-6, IL-9 and IFN-ɤ, which are produced by T-cells, are involved in lupus development in MRL/lpr mice (Tang et al. 1991; Balomenos et al. 1998; Yang et al. 2015). Thus, it is proposed that variations in levels of these cytokines in serum and/or tissues alters the oviductal CBF of MRL/lpr mice. The inflammatory factors affecting CBF may be involved in the complicated regulation of ciliary function in mice, as no significant correlations between the oviductal CBF and oocyte pick-up were found. It is proposed that altered ciliary function triggered by an aberrant immune condition affects the pivotal physiological function of the reproductive tract.

In addition to oviductal cilia, we examined tracheal cilia to evaluate systemic ciliary morphofunction. The tracheal CBF in MRL/lpr decreased with age and correlated negatively with S/B. These results indicate that the progression of the systemic autoimmune abnormality in MRL/lpr mice alters systemic ciliary function, similar to oviductal cilia. However, in contrast to oviductal morphology, the ultrastructure of tracheal ciliated cells did not exhibit any significant changes. The molecular pathogenesis of altered ciliary beating speed can thus be explained by a systemic inflammatory response, while the abnormality of the oviduct cilia ultrastructure seems to involve an additional local pathological response. Female patients with primary ciliary dyskinesia (PCD), the congenital autosomal recessive genetic disorder characterized by total or partial

dysfunction of the ciliary cells due to ciliary ultrastructural abnormalities, largely show such respiratory alterations and sometimes are infertile (Leigh et al. 2009; Armengot et al. 2010). However, some female PCD patients with severely dysfunctional respiratory cilia successfully conceive and deliver babies (Vanaken et al. 2017). The features of ciliary ultrastructural abnormalities in PCD vary in the oviduct and respiratory tract, so it is proposed that the effects of mutated proteins and protein expression would vary in these different tissues (Lurie et al. 1989). Taken together, due to the tissue-related differences in the function and/or expression of disease-associated molecules, the ciliary morphofunction of the oviduct is more susceptible to aging and/or immune abnormalities than the trachea and severely impacts reproductive function in MRL/lpr mice.

We also found histological and functional relationship between the oviductal tract and respiratory tract in mammals. The strong positive correlation between the oviductal and tracheal CBF and ciliary cooperativity gives rise to two theories. The first theory is that the one or more molecules circulating systemically have identical effects on the systemic ciliary function. The second theory is that the inflammatory substances produced by immune cells, such as T-cells, infiltrate into the tissue and alter the ciliary beating patterns, resulting in the systemic decrease of CBF. The clinical reports in women with tubal ectopic pregnancies, which is suspected to be caused by the oviductal ciliary abnormalities, support comparisons between this study and human

pathology. Both oviductal and nasal CBF in those patients correlated positively and was decreased compared with healthy women (Liao et al. 2012; O et al. 2013). The peptide hormone adrenomedullin was reported to be involved in the molecular pathogenesis of tubal ectopic pregnancies and decreased oviductal and nasal CBF. The significant positive correlation between the tracheal CBF and the oocyte pick-up rate in MRL/lpr mice interestingly suggests that changes in the tracheal ciliary beating reflects that of the oviductal reproductive function in mice.

In human patients, ciliary morphofunctional abnormalities are observed after infection and inflammation in both the lower and upper respiratory tract and is referred to as secondary ciliary dyskinesia (Armengot et al. 2010; Shorter et al. 2016). Additionally, in human patients with granulomatosis with polyangiitis, a potentially lethal systemic autoimmune disease characterized by necrotizing vasculitis of small arteries and veins (Kubaisi et al. 2016), the nasal CBF is severely impaired (Ullrich et al. 2009). In the patients with asthma, an inflammatory respiratory disease, both the secondary ciliary dysfunction and the secondary ultrastructural abnormalities of bronchial epithelium are closely related to asthma severity (Thomas et al. 2010). The ciliary ultrastructural abnormalities in patient airways were also reported to be associated with long-lasting airways infections (Corbeel et al. 1981). In the female PCD patients, the immobility of cilia on oviductal epithelial cells leads the oocyte transportation failure (Mccomb et al. 1986). We estimate that the ovulation disorders and oocyte pick-up by oviducts is also involved in the infertility of the patients

with dysfunction of motile cilia.

In conclusion, oocyte pick-up on the oviductal infundibulum is regulated by ciliary function, requires appropriate beating speed and coordinated beating directions and becomes abnormal upon impairment of the local environmental immune balance in ciliated epithelium during systemic autoimmune disease conditions in MRL/lpr mice. We also found a close correlation between the change of ciliary morphofunction in the respiratory tract and that of morphofunction in the reproductive tract.

Acknowledgements

This work was supported in part by JSPS KAKENHI Grant Number JP18J22313 (M. Hosotani). The research described in this paper was presented in part at the 161th Japanese Association of Veterinary Anatomists, 11-13 September 2018 in Ibaraki. We are deeply grateful to Dr. Jason Chen for willingly supporting our CBF measurements by providing us his developed program.

Author contributions

M. Hosotani designed, performed experiments, and analyzed data. M.A. Masum and Y. Otani analyzed data. O. Ichii, T. Nakamura, Y.H.A. Elewa, and Y. Kon designed and reviewed the

experiments. M. Hosotani, O. Ichii, and Y. Kon wrote the manuscript. All authors approved the final manuscript.

Conflicts of Interest

The authors declare no conflicts of interest.

Ethical Approval

Animal experimentation was approved by the Institutional Animal Care and Use Committee of the Graduate School of Veterinary Medicine, Hokkaido University (Approval No. 15-0079). Experimental animals were handled in accordance with the Guide for the Care and Use of Laboratory Animals, Graduate School of Veterinary Medicine, Hokkaido University (approved by the Association for Assessment and Accreditation of Laboratory Animal Care International).

References

Andrews BS, Eisenberg RA, Theofilopoulos AN, et al (1978) Spontaneous murine lupus-like syndromes. Clinical and immunopathological manifestations in several strains. J Exp Med 148:1198–215

Ardighieri L, Lonardi S, Moratto D, et al (2014) Characterization of the immune cell repertoire in the normal fallopian tube. Int J Gynecol Pathol 33:581–91. https://doi.org/10.1097/PGP.0000000000000095

Armengot M, Milara J, Mata M, et al (2010) Cilia motility and structure in primary and secondary ciliary dyskinesia. Artic Am J Rhinol Allergy 24:175–180. https://doi.org/10.2500/ajra.2010.24.3448

Avasthi P, Marshall WF (2012) Stages of ciliogenesis and regulation of ciliary length. Differentiation 83:S30–S42. https://doi.org/10.1016/J.DIFF.2011.11.015

Balomenos D, Rumold R, Theofilopoulos AN (1998) Interferon-ɤ is Required for Lupus-like Disease and Lymphoaccumulation in MRL-lpr Mice. J Clin In-vest 101:364–371

Carp HJA, Selmi C (2012) The autoimmune bases of infertility and pregnancy loss. J Autoimmun 38:J266–J274. https://doi.org/10.1016/J.JAUT.2011.11.016

Chen JJ, Lemieux BT, Wong BJF (2016) A Low-Cost Method of Ciliary Beat Frequency Measurement Using iPhone and MATLAB. Otolaryngol - Head Neck Surg (United States) 155:252–256. https://doi.org/10.1177/0194599816640219

Corbeel L, Cornillie F, Lauweryns J, et al (1981) Ultrastructural abnormalities of bronchial cilia in children with recurrent airway infections and bronchiectasis. Arch Dis Child 56:929–33. https://doi.org/10.1136/ADC.56.12.929

Crow J, Amso NN, Lewin J, Shaw RW (1994) Morphology and ultrastructure of fallopian tube epithelium at different stages of the menstrual cycle and menopause. Hum Reprod 9:2224–

2233. https://doi.org/10.1093/oxfordjournals.humrep.a138428

Dummer A, Rol N, Szulcek R, et al (2018) Endothelial dysfunction in pulmonary arterial hypertension: loss of cilia length regulation upon cytokine stimulation. Pulm Circ 8:1–9. https://doi.org/10.1177/2045894018764629

Elewa YHA, Ichii O, Kon Y (2017) Sex-related differences in autoimmune-induced lung lesions in MRL/MpJ- *fas* ^{lpr} mice are mediated by the development of mediastinal fat-associated lymphoid clusters. Autoimmunity 50:306–316. https://doi.org/10.1080/08916934.2017.1344973

Fang X, Zaman MH, Guo X, et al (2018) Role of Hepatic Deposited Immunoglobulin G in the Pathogenesis of Liver Damage in Systemic Lupus Erythematosus. Front Immunol 9:1457. https://doi.org/10.3389/fimmu.2018.01457

Gordts S, Campo R, Rombauts L, Brosens I (1998) Endoscopic visualization of the process of fimbrial ovum retrieval in the human. Hum Reprod 13:1425–1428. https://doi.org/10.1093/humrep/13.6.1425

Grosse-Onnebrink J, Werner C, Loges NT, et al (2016) Effect of TH2 cytokines and interferon gamma on beat frequency of human respiratory cilia. Pediatr Res 79:731–735. https://doi.org/10.1038/pr.2016.8

Guirao B, Meunier A, Mortaud S, et al (2010) Coupling between hydrodynamic forces and planar cell polarity orients mammalian motile cilia. Nat Cell Biol 12:341–350. https://doi.org/10.1038/ncb2040

Haller-Kikkatalo K, Salumets A, Uibo R (2012) Review on autoimmune reactions in female infertility: antibodies to follicle stimulating hormone. Clin Dev Immunol 2012:762541. https://doi.org/10.1155/2012/762541

Hosotani M, Ichii O, Nakamura T, et al (2018) Autoimmune abnormality affects ovulation and

499 oocyte-pick-up in MRL/MpJ-Fas lpr/lpr mice. Lupus 27:82–94.
500 https://doi.org/10.1177/0961203317711772
501 Huang S, Driessen N, Knoll M, Talbot P (1997) In Vitro Analysis of Oocyte Cumulus Complex
502 Pickup Rate in the Hamster Mesocricetus auratus. Mol Reprod Dev 47:312–322
503 Ichii O, Otsuka S, Sasaki N, et al (2010) Local overexpression of interleukin-1 family, member 6
504 relates to the development of tubulointerstitial lesions. Lab Investig 90:459–475.
505 https://doi.org/10.1038/labinvest.2009.148
506 Iwasaki A, Foxman EF, Molony RD (2017) Early local immune defences in the respiratory tract.
507 Nat Rev Immunol 17:7–20. https://doi.org/10.1038/nri.2016.117
508 Kanno H, Nose M, Itoh J, et al (1992) Spontaneous development of pancreatitis in the MRL/Mp
509 strain of mice in autoimmune mechanism. Clin Exp Immunol 89:68–73
510 Klettke U, Luck W, Wahn U, Niggemann B (1999) Platelet-activating factor inhibits ciliary beat
511 frequency of human bronchial epithelial cells. Allergy asthma Proc 20:115–8
512 Kubaisi B, Samra KA, Foster CS (2016) Granulomatosis with polyangiitis (Wegener's disease):
513 An updated review of ocular disease manifestations. Intractable Rare Dis Res 5:61–69.
514 https://doi.org/10.5582/IRDR.2016.01014
515 Leigh MW, Pittman JE, Carson JL, et al (2009) Clinical and Genetic Aspects of Primary Ciliary
516 Dyskinesia / Kartagener Syndrome. Genet Med 11:473–487.
517 https://doi.org/10.1097/GIM.0b013e3181a53562
518 Liao SB, Li HWR, Ho JC, et al (2012) Possible Role of Adrenomedullin In the Pathogenesis of
519 Tubal Ectopic Pregnancy. J Clin Endocrinol Metab 97:2105–2112.
520 https://doi.org/10.1210/jc.2011-3290
521 Luborsky J (2002) Ovarian Autoimmune Disease and Ovarian Autoantibodies. J Womens Health
522 Gend Based Med 11:585–599

523 Lurie M, Tur-Kaspa I, Weill S, et al (1989) Ciliary Ultrastructure of Respiratory and Fallopian
524 Tube Epithelium in a Sterile Woman with Kartagener's Syndrome: A Quantitative
525 Estimation. Chest 95:578–581. https://doi.org/10.1378/CHEST.95.3.578
526 Magdy N, El-Bahrawy M (2014) Fallopian tube: Its role in infertility and gynecological
527 oncology. World J Obstet Gynecol 3:35–41. https://doi.org/10.5317/wjog.v3.i2.35
528 Mccomb P, Langley L, Sd M, Verdugo P (1986) The oviductal cilia and Kartagener's syndrome.
529 Fertil Steril 46:412–416. https://doi.org/10.1016/S0015-0282(16)49578-6
530 Nagata Y, Ichikawa T, Oakda H, et al (2004) Views of Infertile Patients on Application of
531 Assisted Reproductive Technologies for Extra-marital State. J Fertil Implant 21:6–14
532 Niwa S, Nakajima K, Miki H, et al (2012) KIF19A Is a Microtubule-Depolymerizing Kinesin for
533 Ciliary Length Control. Dev Cell 23:1167–1175.
534 https://doi.org/10.1016/J.DEVCEL.2012.10.016
535 Norwood JT, Hein CE, Halbertt SA, Anderson RGW (1978) Polycationic macromolecules
536 inhibit cilia-mediated ovum transport in the rabbit oviduct. Cell Biol 75:4413–4416
537 O WS, Li HWR, Liao S-B, et al (2013) Decreases in adrenomedullin expression and ciliary beat
538 frequency in the nasal epithelium in tubal pregnancy. Fertil Steril 100:459-463.e1.
539 https://doi.org/10.1016/J.FERTNSTERT.2013.04.007
540 Otani Y, Ichii O, Otsuka-Kanazawa S, et al (2015) MRL/MpJ- *Fas* ^{lpr} mice show abnormalities
541 in ovarian function and morphology with the progression of autoimmune disease.
542 Autoimmunity 48:402–411. https://doi.org/10.3109/08916934.2015.1031889
543 Papathanasiou A, Djahanbakhch O, Saridogan E, Lyons RA (2008) The effect of interleukin-6
544 on ciliary beat frequency in the human fallopian tube. Fertil Steril 90:391–394.
545 https://doi.org/10.1016/j.fertnstert.2007.07.1379
546 Peters WM (1986) Nature of "basal" and "reserve" cells in oviductal and cervical epithelium in

547 man. J Clin Pathol 39:306–12. https://doi.org/10.1136/jcp.39.3.306
548 Rautiainen M, Collan Y, Nuutinen J (1986) A method for measuring the orientation (“beat
549 direction”) of respiratory cilia. Arch Otorhinolaryngol 243:265–268
550 Roupa Z, Polikandrioti M, Sotiropoulou P, et al (2009) Causes of infertility in women at
551 reproductive age. A Dr Z Roupa Aigosthenon 3:80–87
552 Santiago-Raber M-L, Laporte C, Reininger L, Izui S (2004) Genetic basis of murine lupus.
553 Autoimmun Rev 3:33–39. https://doi.org/10.1016/S1568-9972(03)00062-4
554 Sawamukai Y, Minami Y, Nakano T, De Silva LNA (2014) Tubal Patency and Fertility in
555 Repeat Breeder cows. J Japan Vet Med Assoc 50:224–227.
556 https://doi.org/10.12935/jvma1951.50.224
557 Sen A, Kushnir VA, Barad DH, Gleicher N (2014) Endocrine autoimmune diseases and female
558 infertility. Nat Rev Endocrinol 10:37–50. https://doi.org/10.1038/nrendo.2013.212
559 Shi D, Komatsu K, Uemura T, Fujimori T (2011) Analysis of ciliary beat frequency and ovum
560 transport ability in the mouse oviduct. Genes to Cells 16:282–290.
561 https://doi.org/10.1111/j.1365-2443.2011.01484.x
562 Shorter SL, Albaghdadi AJH, Kan FWK (2016) Alterations in oviductal cilia morphology and
563 reduced expression of axonemal dynein in diabetic NOD mice. Tissue Cell 48:588–595.
564 https://doi.org/10.1016/J.TICE.2016.10.003
565 Takeo T, Hoshii T, Kondo Y, et al (2008) Methyl-Beta-Cyclodextrin Improves Fertilizing
566 Ability of C57BL/6 Mouse Sperm after Freezing and Thawing by Facilitating Cholesterol
567 Efflux from the Cells1. Biol Reprod 78:546–551.
568 https://doi.org/10.1095/biolreprod.107.065359
569 Tang B, Matsuda T, Akira S, et al (1991) Age-associated increase in interleukin 6 in MRL/lpr
570 mice. Int Immunol 3:273–278. https://doi.org/10.1093/intimm/3.3.273

571 Thomas B, Rutman A, Hirst RA, et al (2010) Ciliary dysfunction and ultrastructural
572 abnormalities are features of severe asthma. J Allergy Clin Immunol 126:722-729.e2.
573 https://doi.org/10.1016/j.jaci.2010.05.046
574 Ullrich S, Gustke H, Lamprecht P, et al (2009) Severe impaired respiratory ciliary function in
575 Wegener granulomatosis. Ann Rheum Dis 69:1067–1071.
576 https://doi.org/10.1136/ard.2008.096974
577 Vanaken GJ, Bassinet L, Boon M, et al (2017) Infertility in an adult cohort with primary ciliary
578 dyskinesia: phenotype-gene association. Eur Respir J 50:1700314.
579 https://doi.org/10.1183/13993003.00314-2017
580 Yang J-Q, Saxena V, Xu H, et al (2003) Repeated α-Galactosylceramide Administration Results
581 in Expansion of NK T Cells and Alleviates Inflammatory Dermatitis in MRL-lpr/lpr Mice. J
582 Immunol 171:4439–4446. https://doi.org/10.4049/jimmunol.171.8.4439
583 Yang J, Li Q, Yang X, Li M (2015) Interleukin-9 Is Associated with Elevated Anti-Double-
584 Stranded DNA Antibodies in Lupus-Prone Mice. Mol Med 21:364–70.
585 https://doi.org/10.2119/molmed.2014.00237
586

FIGURE LEGENDS

Figure 1. Indices of autoimmune abnormality, ovulation, and oocyte pick-up in MRL/+ and MRL/lpr mice.

(a) Ratio of spleen weight to body weight (S/B ratio). n = 4, 4, 6 and 7.

(b) The concentration of serum anti-double-stranded DNA (anti-dsDNA) antibody. n = 4, 4, 6 and 8.

(c) Number of cumulus oocyte complexes (COCs). n = 8, 8, 8 and 11.

(d) Number of ovulated oocytes (OOs) in ovarian serial sections. n = 7, 7, 8 and 11.

(e) Oocyte pick-up ratio (PUR) calculated from values in (c) and (d). n = 7, 7, 8 and 11.

Data are mean ± s.e.m. **P* < 0.05, ***P* < 0.01, ****P* < 0.001 (Mann-Whitney *U*-test). n values are listed in the following order: 3-month-old MRL/+ mice, 3-month-old MRL/lpr mice, 6-month-old MRL/+ mice, and 6-month-old MRL/lpr mice. MRL/+ = MRL/MpJ; MRL/lpr = MRL/MpJ-*Fas*$^{lpr/lpr}$.

Figure 2. The histology and cilia beating in the ciliated epithelial cells in the oviductal infundibulum

(a-a’’’) Histological sections of the oviductal infundibulum stained with hematoxylin-eosin. Arrowheads indicate secretory cells. Bar = 25μm.

(b-b’’’) Localization of CD-3 positive T-cells in the oviductal infundibulum as revealed by immunohistochemistry. Bar = 100 μm.

(c-c’’’) The sequential ciliary beating patterns observed by stereo microscopy. Arrowheads indicate the same cilia in multiple frames. (a, b, c), (a’, b’, c’), (a’’, b’’, c’’) and (a’’’, b’’’, c’’’) show the oviductal images of 3-month-old MRL/+ mice, 3-month-old MRL/lpr mice, 6-month-old MRL/+ mice, and 6-month-old MRL/lpr mice, respectively.

(d) Oviductal ciliary beating frequency (CBF). n = 7, 7, 8, 11. Data are mean ± s.e.m. $^{**}P < 0.01$ (Mann-Whitney *U*-test). n values are listed in the following order: 3-month-old MRL/+ mice, 3-month-old MRL/lpr mice, 6-month-old MRL/+ mice, and 6-month-old MRL/lpr mice. MRL/+ = MRL/MpJ; MRL/lpr = MRL/MpJ-$Fas^{lpr/lpr}$.

Figure 3. The ultrastructure of cilia of the ciliated epithelial cells in the oviductal infundibulum.

The oviductal ciliary ultrastructure as observed by transmission electron microscopy (TEM). The white bidirectional arrows indicate the ciliary height. The ciliary height on the oviductal ciliated epithelial cells in the HE-stained sections is shown as black lines in the insets of (a), (c), (e) and (g). The white lines are drawn through central pairs of microtubules located at the center of cilia. Bar = 500 nm. (a, b), (c, d), (e, f) and (g, h) show the ultrastructural sections of 3-month-old MRL/+

623 mice, 3-month-old MRL/lpr mice, 6-month-old MRL/+ mice, and 6-month-old MRL/lpr mice,

624 respectively. MRL/+ = MRL/MpJ; MRL/lpr = MRL/MpJ-*Fas*$^{lpr/lpr}$.

625

626 **Figure 4. The indices of the ultrastructural changes in the cilia of the oviductal infundibulum.**

627 (a) The oviductal ciliary height. n = 4 per group.

628 (b) Oviductal ciliary cooperativity of the beating direction is shown as mean vector length (r_{cell}).

629 n = 4 per group.

630 Data are the mean ± s.e.m. *P < 0.05 (Mann-Whitney U-test). MRL/+ = MRL/MpJ; MRL/lpr =

631 MRL/MpJ-*Fas*$^{lpr/lpr}$.

632

633 **Figure 5. The histology and beating of cilia on the ciliated epithelial cells in the trachea.**

634 (a-a’’’) The histology of the trachea. Arrowheads indicate non-ciliated cells. Arrows indicate mucin

635 layer. Dashed line indicates the region of infiltrated mononuclear cells. Hematoxylin-eosin stained.

636 Bar = 50 μm.

637 (b-b’’’) The localization of CD-3 positive T-cells in the trachea revealed by immunohistochemistry.

638 Bar = 50 μm.

639 (c-c’’’) The sequential ciliary beating pattern observed by stereo microscopy. Arrowheads indicate

640 the same cilia in multiple frames. (a, b, c), (a’, b’, c’), (a’’, b’’, c’’) and (a’’’, b’’’, c’’’) show the

tracheal images of 3-month-old MRL/+ mice, 3-month-old MRL/lpr mice, 6-month-old MRL/+ mice, and 6-month-old MRL/lpr mice, respectively.

(d) The trachea ciliary beating frequency (CBF). n = 4, 4, 6, 7. Data are the mean ± s.e.m. *P < 0.05 (Mann-Whitney U-test). n values are listed in the following order: 3-month-old MRL/+ mice, 3-month-old MRL/lpr mice, 6-month-old MRL/+ mice, and 6-month-old MRL/lpr mice. MRL/+ = MRL/MpJ; MRL/lpr = MRL/MpJ-*Fas*$^{lpr/lpr}$.

Figure 6. The ultrastructure of cilia of the ciliated epithelial cells in the trachea.

The tracheal ciliary ultrastructure as observed by transmission electron microscopy (TEM). The black bidirectional arrows indicate the ciliary height. The ciliary height on the tracheal ciliated epithelial cells in the HE-stained sections is shown as black lines in the insets of (a), (c), (e) and (g).The white lines are drawn through central pairs of microtubules located at the center of cilia. Bar = 500 nm. (a, b), (c, d), (e, f) and (g, h) show the ultrastructural sections of 3-month-old MRL/+ mice, 3-month-old MRL/lpr mice, 6-month-old MRL/+ mice, and 6-month-old MRL/lpr mice, respectively. MRL/+ = MRL/MpJ; MRL/lpr = MRL/MpJ-*Fas*$^{lpr/lpr}$.

Figure 7. The indices of the ultrastructural changes in the cilia of the trachea.

(a) Tracheal ciliary height. n = 4 per group.

(b) The tracheal ciliary cooperativity of beating direction is shown as the mean vector length (r_{cell}). n = 4 per group.

Data are the mean ± s.e.m. MRL/+ = MRL/MpJ; MRL/lpr = MRL/MpJ-*Fas*$^{lpr/lpr}$.

Supplementary Figure S1. Scheme of the preparation for the ciliary beat frequency measurement.

(a) Oviductal infundibulum preparation schematic. The infundibulum is placed into the drop of D-MEM (high glucose) with L-Glutamine and phenol red (D-MEM) and covered with a cover slip so that the ciliated epithelium faces the cover slip.

(b) Trachea preparation schematic. The pieces of trachea are placed into D-MEM on a slide and sealed with a cover slip.

Online Resource 1. The ciliary beating in the oviductal infundibulum of MRL/MpJ mice at 3 months.

Online Resource 2. The ciliary beating in the oviductal infundibulum of MRL/MpJ mice at 6 months.

Online Resource 3. The ciliary beating in the oviductal infundibulum of MRL/MpJ-*Fas*$^{lpr/lpr}$ mice at 3 months.

Online Resource 4. The ciliary beating in the oviductal infundibulum of MRL/MpJ-*Fas*$^{lpr/lpr}$ mice at 6 months.

Online Resource 5. The ciliary beating in the trachea of MRL/MpJ mice at 3 months.

Online Resource 6. The ciliary beating in the trachea of MRL/MpJ mice at 6 months.

Online Resource 7. The ciliary beating in the trachea of MRL/MpJ-*Fas*$^{lpr/lpr}$ mice at 3 months.

Online Resource 8. The ciliary beating in the trachea of MRL/MpJ-*Fas*$^{lpr/lpr}$ mice at 6 months.

685 **Table 1. Spearman's correlation coefficient (ρ) between oocyte-pick-up and ovulation.**

		Parameters	
	Strains	*COCs*	*OOs*
PUR	All mice	0.547**	0.416*
	MRL/+	0.212	-0.156
	MRL/lpr	0.641**	0.563*

*$P < 0.05$; **$P < 0.01$; MRL/+: MRL/MpJ; MRL/lpr: MRL/MpJ-Fas$^{lpr/lpr}$; PUR: oocyte pick-up rate; COCs: cumulus oocyte complexes; OOs: ovulated oocytes.

686

Table 2. Spearman's correlation coefficient (ρ) between the oviductal or tracheal ciliary beat frequency and the indices of the autoimmune disease, ovulation or oocyte-pick-up function.

		Parameters					
	Strains	*S/B*	*Anti-dsDNA antibody*	*COCs*	*OOs*	*PUR*	*Oviductal CBF*
Oviductal	All mice	0.391*	0.507**	0.241	0.231	0.019	-
CBF	MRL/+	-0.255	-0.165	0.530*	0.349	0.463	-
	MRL/lpr	-0.489*	0.008	0.720***	0.727***	0.425	-
Tracheal	All mice	-0.447	-0.195	0.686***	0.749***	0.382**	0.249
CBF	MRL/+	-0.083	-0.333	-0.356	-0.171	-0.189	-0.058
	MRL/lpr	-0.649*	0.115	0.844***	0.825***	0.637**	0.636**

*P < 0.05; **P < 0.01; ***P < 0.001; MRL/+ = MRL/MpJ; MRL/lpr = MRL/MpJ-*Fas*$^{lpr/lpr}$; CBF: ciliary beat frequency; S/B: ratio of spleen weight to body weight; Anti-dsDNA: anti-double-stranded DNA; COCs: cumulus oocyte complexes; OOs: ovulated oocyte; PUR: oocyte pick-up rate.

690 **Table 3. Spearman's correlation coefficients (ρ) between the oviductal and tracheal**

691 **ultrastructure and the ratio of spleen weight to body weight.**

		Parameters		
	Strains	*S/B*	*Oviductal r_{cell}*	*Oviductal ciliary height*
Oviductal r_{cell}	All mice	-0.482	-	-
	MRL/+	0.036	-	-
	MRL/lpr	-0.590	-	-
Tracheal r_{cell}	All mice	-0.351	0.3879	-
	MRL/+	0.381	-0.108	-
	MRL/lpr	-0.483	0.952^{**}	-
Oviductal ciliary height	All mice	0.077	-	-
	MRL/+	-0.771^{*}	-	-
	MRL/lpr	0.570	-	-
Tracheal ciliary height	All mice	0.024	-	-0.318
	MRL/+	0.500	-	-0.313
	MRL/lpr	-0.524	-	-0.147

*P < 0.05; **P < 0.01; MRL/+ = MRL/MpJ; MRL/lpr = MRL/MpJ-*Fas*$^{lpr/lpr}$; S/B: ration of spleen to body weight.

692

a

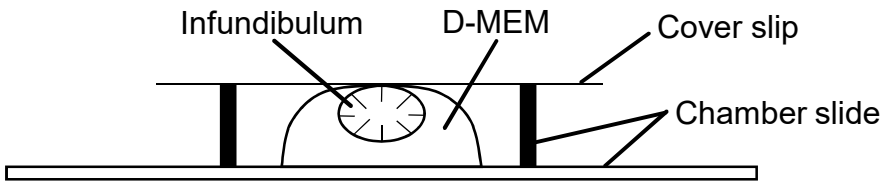
Infundibulum
D-MEM
Cover slip
Chamber slide

b

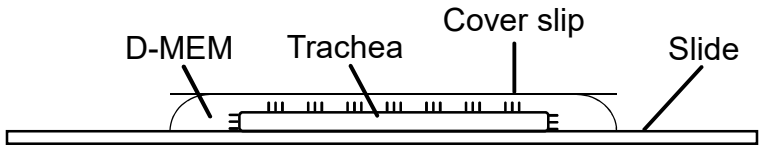
D-MEM
Trachea
Cover slip
Slide

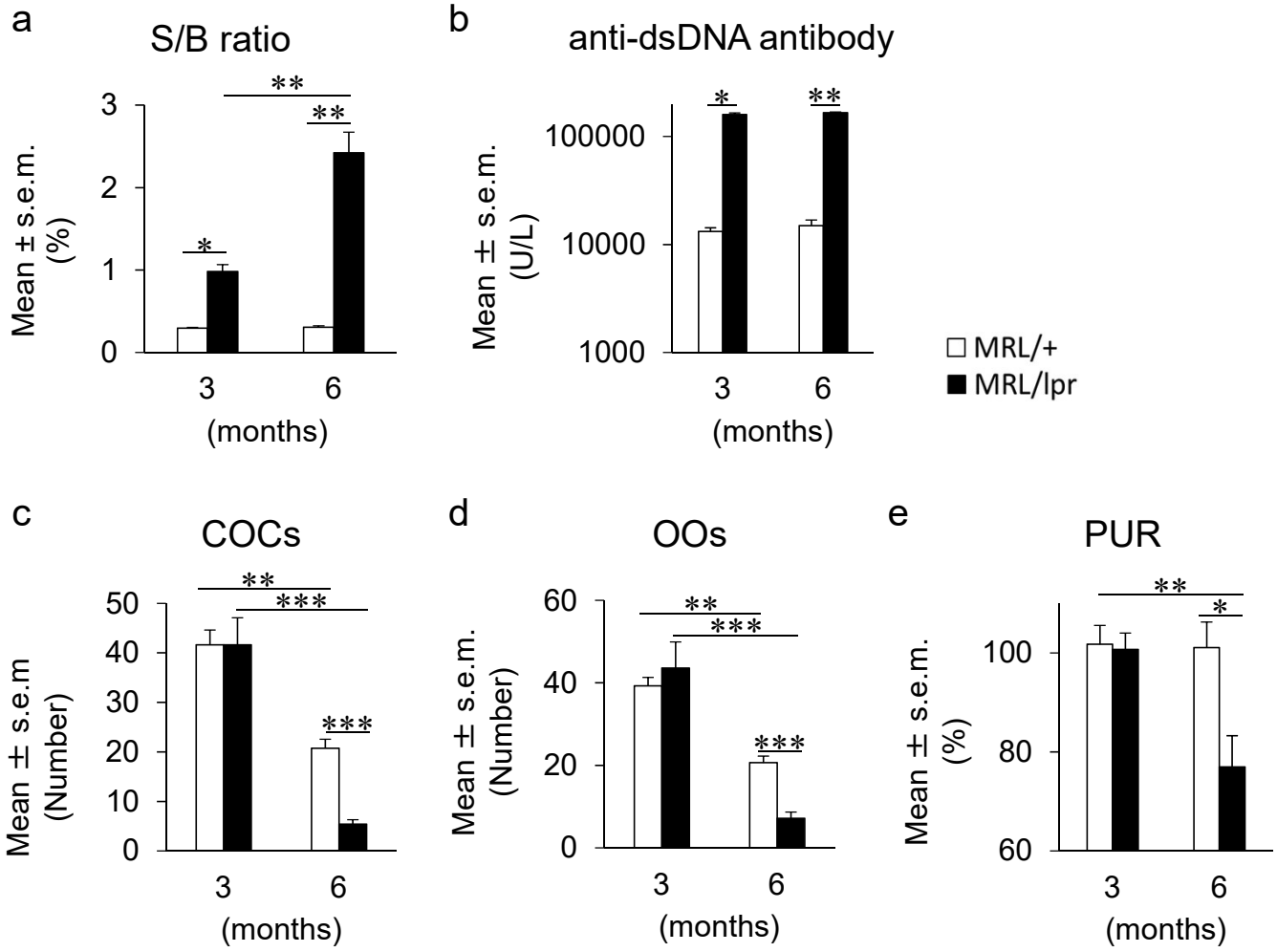
a
S/B ratio
Mean ± s.e.m. (%)
3
2
1
0
**
**
*
3
6
(months)
b
anti-dsDNA antibody
Mean ± s.e.m. (U/L)
100000
10000
1000
*
**
3
6
(months)
□ MRL/+
■ MRL/lpr
c
COCs
Mean ± s.e.m (Number)
50
40
30
20
10
0
**
***
***
3
6
(months)
d
OOs
Mean ± s.e.m. (Number)
60
40
20
0
**
***
***
3
6
(months)
e
PUR
Mean ± s.e.m. (%)
100
80
60
**
*
3
6
(months)

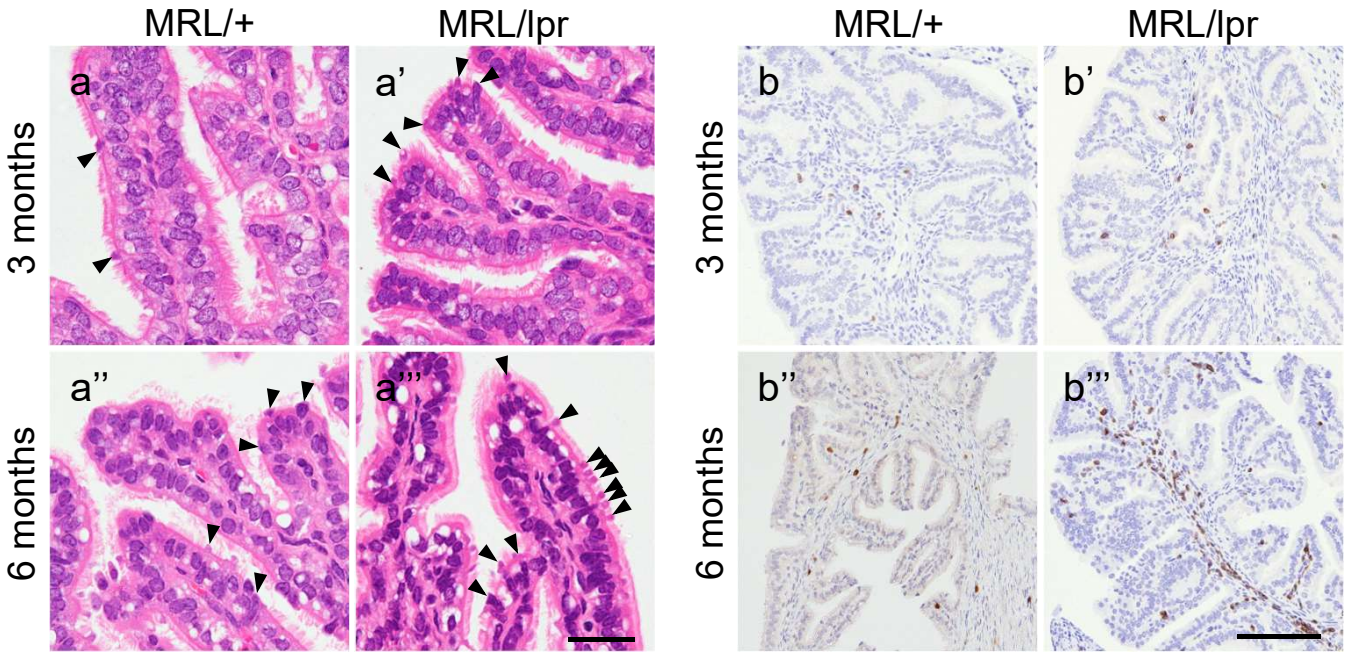
MRL/+
MRL/lpr
3 months
6 months
a
a'
a''
a'''
b
b'
b''
b'''

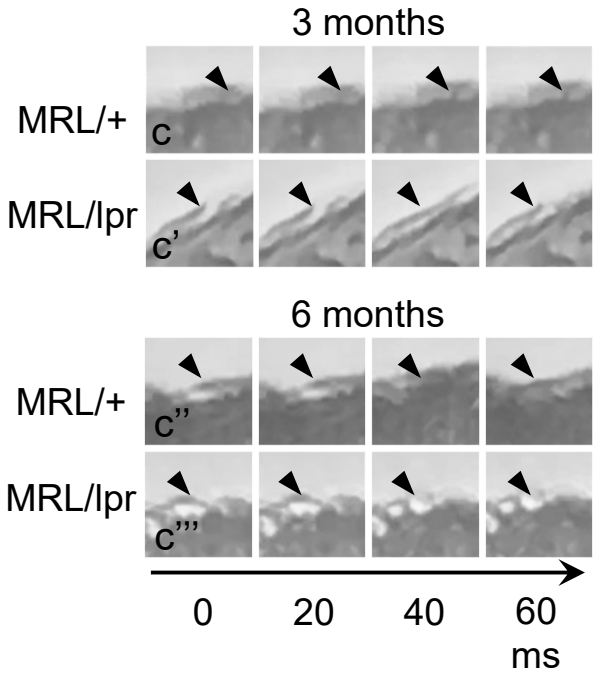
3 months
MRL/+
MRL/lpr
c
c'
6 months
MRL/+
MRL/lpr
c''
c'''
0
20
40
60
ms

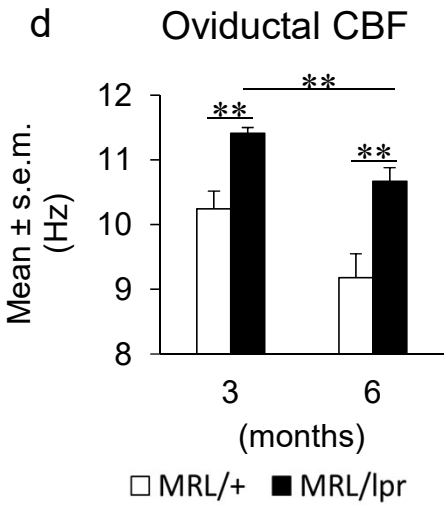
d
Oviductal CBF
Mean ± s.e.m. (Hz)
12
11
10
9
8
**
**
**
3
6
(months)
MRL/+
MRL/lpr

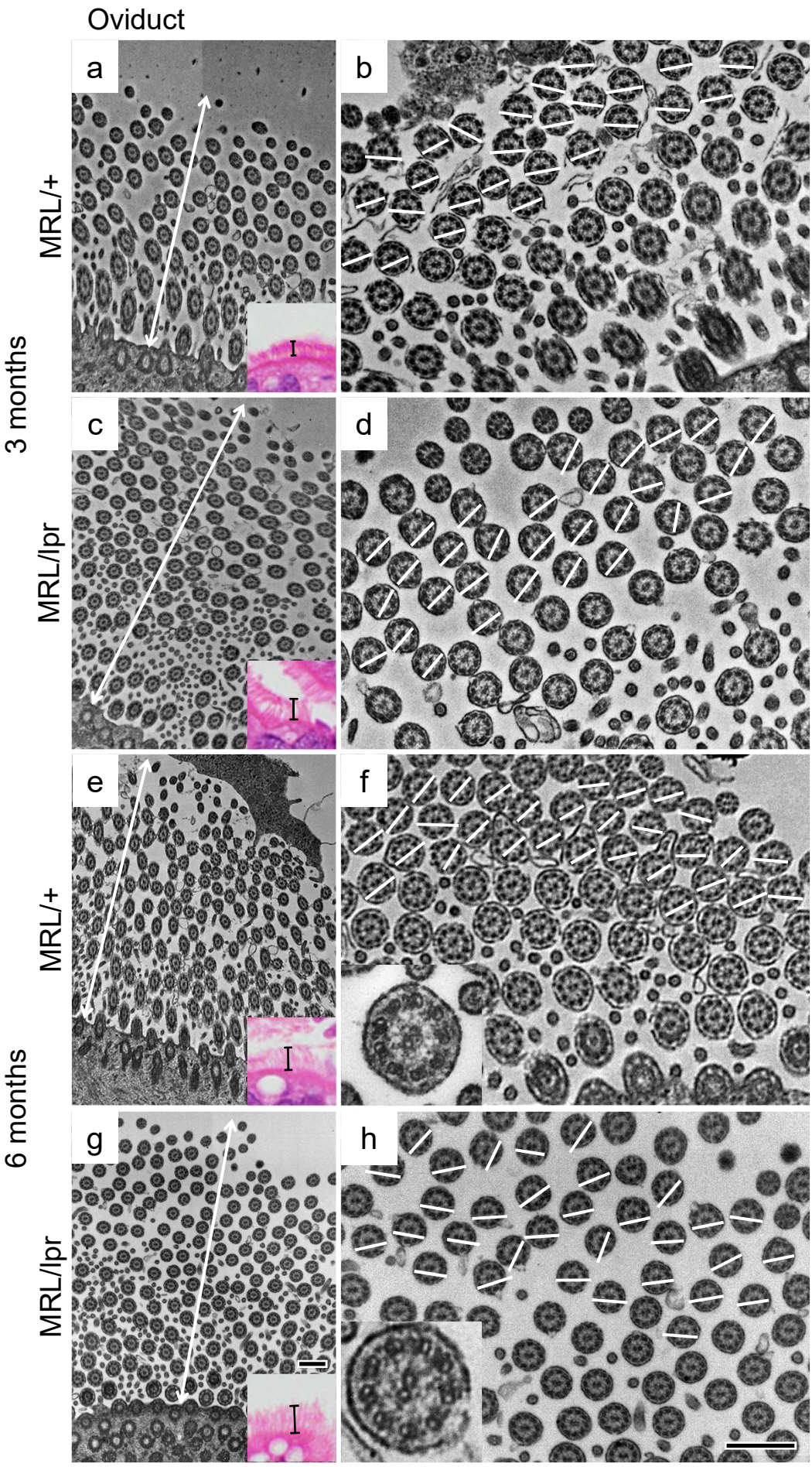
Oviduct
3 months
6 months
MRL/+
MRL/lpr
MRL/+
MRL/lpr
a
b
c
d
e
f
g
h

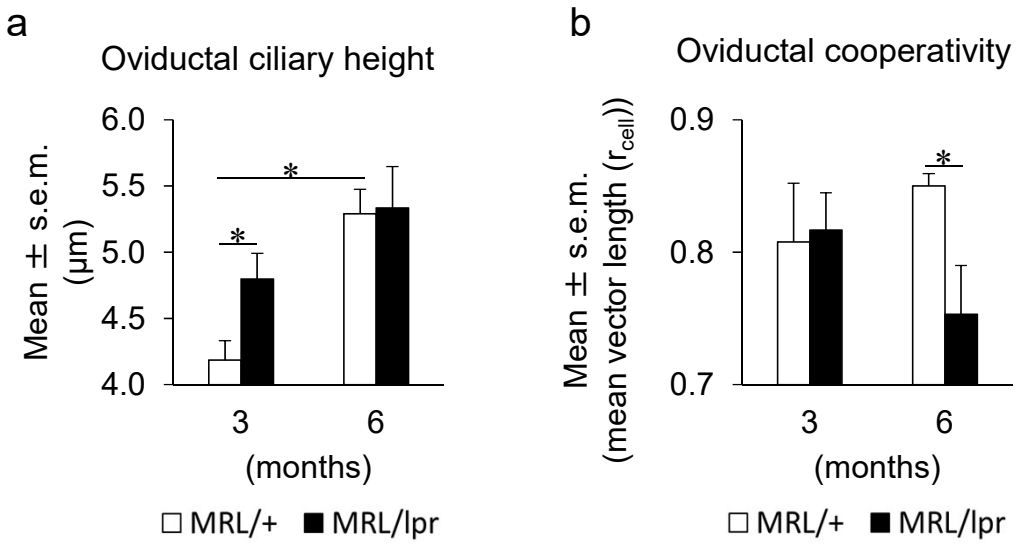
a
Oviductal ciliary height
Mean ± s.e.m. (μm)
6.0
5.5
5.0
4.5
4.0
*
*
3
6
(months)
□ MRL/+ ■ MRL/lpr
b
Oviductal cooperativity
Mean ± s.e.m. (mean vector length (r_{cell}))
0.9
0.8
0.7
*
3
6
(months)
□ MRL/+ ■ MRL/lpr

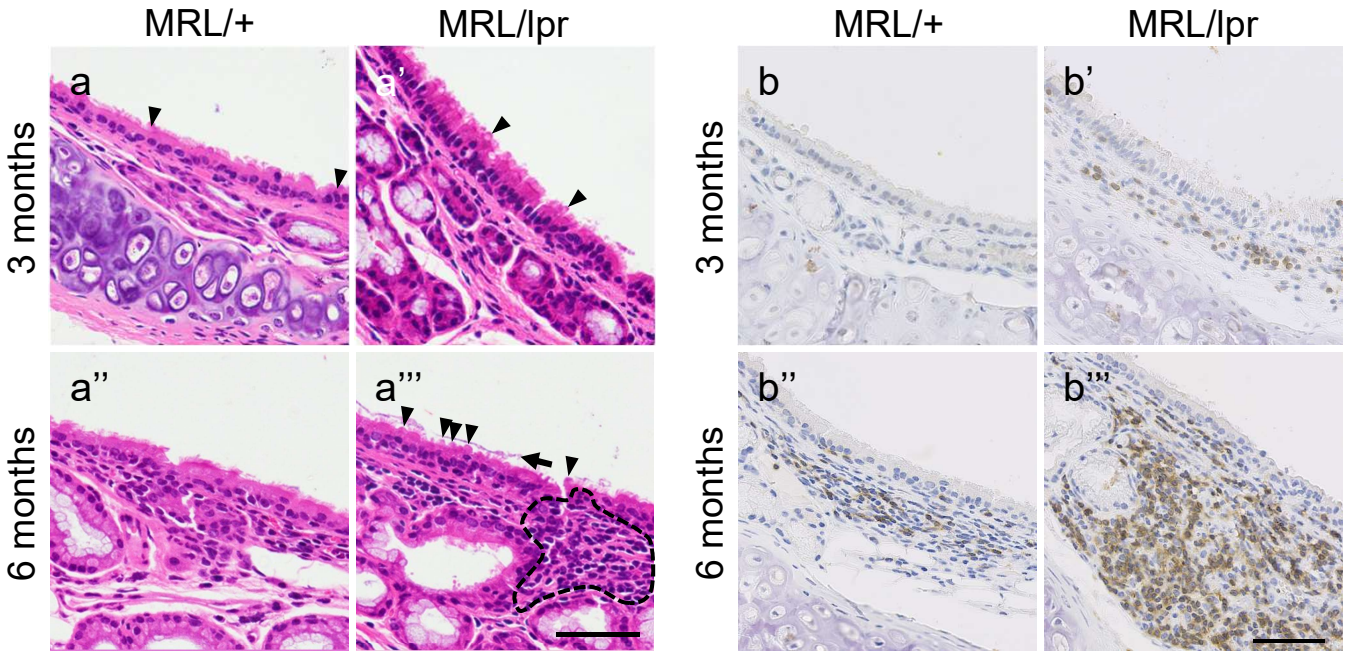
MRL/+
MRL/lpr
3 months
6 months
a
a'
a''
a'''
b
b'
b''
b'''

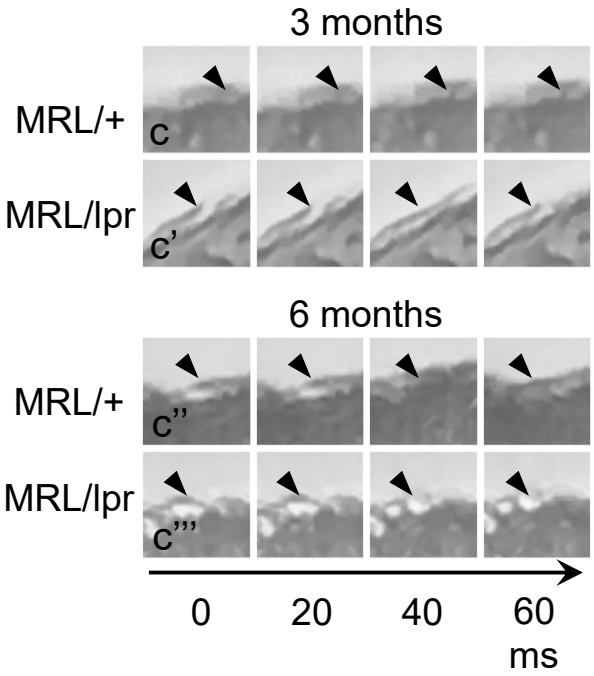
3 months
MRL/+
MRL/lpr
c
c'
6 months
c''
c'''
0
20
40
60
ms

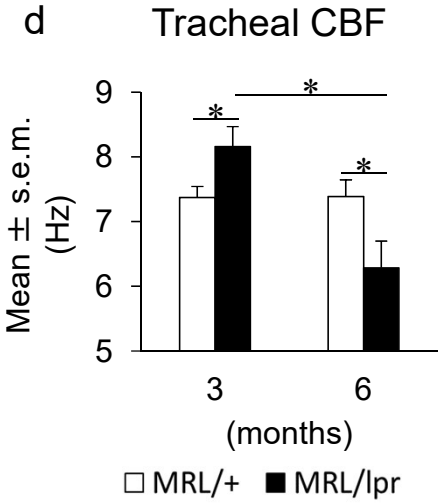
d
Tracheal CBF
Mean ± s.e.m. (Hz)
9
8
7
6
5
3
6
(months)
MRL/+
MRL/lpr
*
*
*

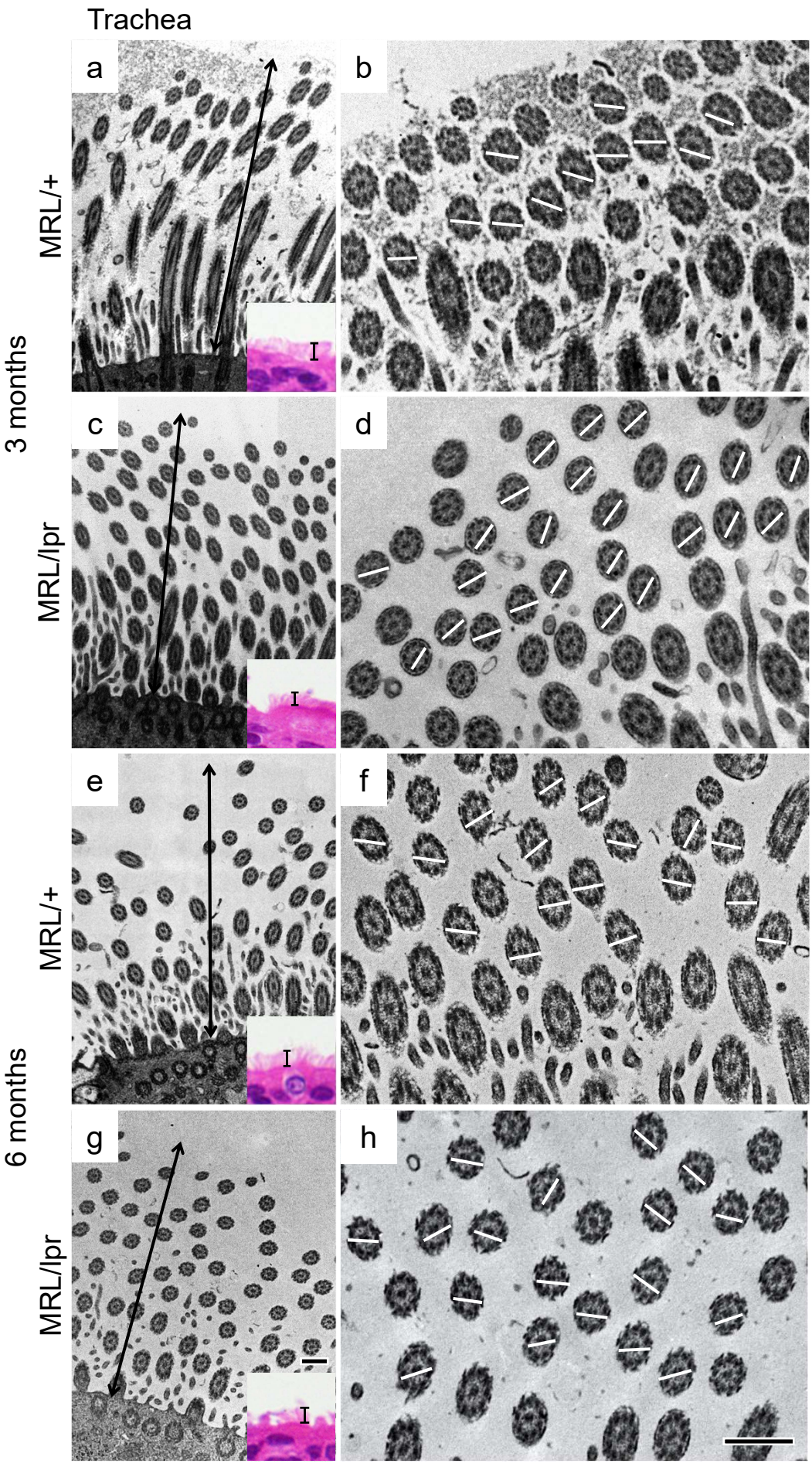
Trachea
3 months
6 months
MRL/+
MRL/lpr
MRL/+
MRL/lpr
a
b
c
d
e
f
g
h

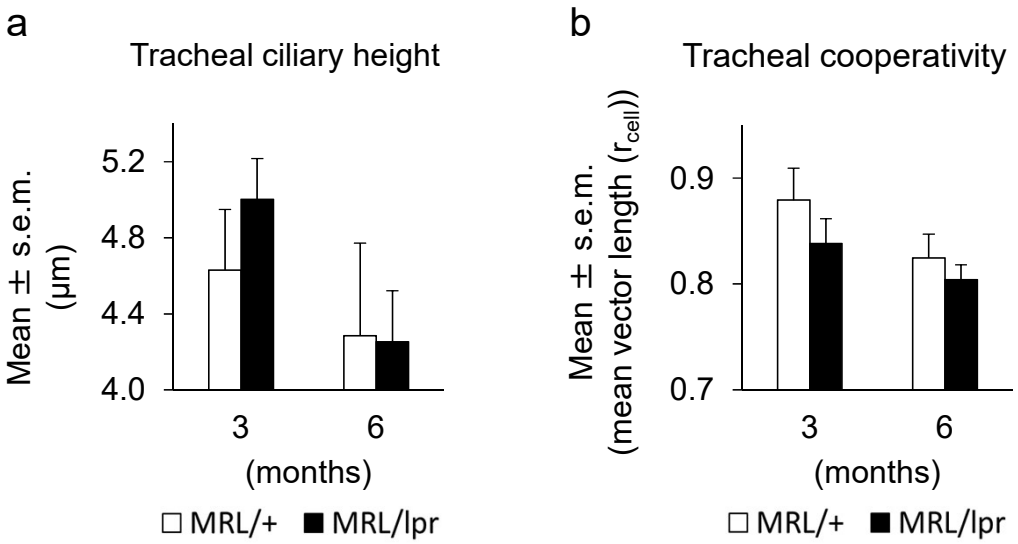
a
Tracheal ciliary height
Mean ± s.e.m. (μm)
5.2
4.8
4.4
4.0
3
6
(months)
□ MRL/+ ■ MRL/lpr
b
Tracheal cooperativity
Mean ± s.e.m. (mean vector length (r_cell))
0.9
0.8
0.7
3
6
(months)
□ MRL/+ ■ MRL/lpr